International Journal of Mathematical Archive-12(7), 2021, 10-21
Available online through www.ijma.info ISSN 2229 – 5046

A COMPARATIVE STUDY OF UNSTEADY FLOW OF NON-NEWTONIAN FLUIDS THROUGH AN INCLINED STENOSED ARTERY

Dr. CHHAMA AWASTHI*

**Department of Mathematics,*
Dr. APJ Abdul Kalam Technical University, **Lucknow-226031, Uttar Pradesh, India.**

(Received On: 04-07-21; Revised & Accepted On: 21-07-21)

ABSTRACT

This investigation accomplishes the comparison of different non-Newtonian fluids such as Bingham Plastic, Herschel Bulkley, and Casson fluid flowing through an inclined stenosed artery. Details of flow characteristics of Bingham Plastic, Casson fluids along with the body acceleration, slip condition at the stenosed wall and asymmetric stenosis effect have been discussed in this paper while Siddiqui and Chhama [10] data has been used for Herschel Bulkley fluid. A comparison of flow quantities like plug core velocity, plug core radius, axial velocity, and effective viscosity has been investigated under the various rheological factors such as yield stress, inclination, stenosis size effect, slip, and body acceleration for different non- Newtonian fluids. It has been found that the axial velocity of Herschel Bulkley fluid is greater than Casson fluid and lower than Bingham Plastic fluid in normal as well as in stenosed artery while in core region where yield stress is more than wall shear stress, plug core velocity of Bingham Plastic fluid is more than that of Casson fluid and less than that of Herschel Bulkley fluid.

Keywords — *Blood, Bingham Plastic fluid, Casson fluid, Herschel Bulkley fluid, Stenosis, Plug core radius, Plug core velocity.*

I. INTRODUCTION

The circulatory flow inside the human body plays an eminent role in blood flow rheology. All body organs are influenced by the pattern of blood flow in the blood vessels under the circulatory system. Atherosclerosis (or stenosis) is a cardiovascular disorder that develops due to the abnormal blood flow in arteries during circulatory disorder. In the stenosis, the artery narrowed due to the presence of plaques inside the arterial wall. Therefore, blood flow is obstructed inside the artery. An unsteady flow of blood via a stenosed artery, assuming the blood to be Herschel-Bulkley fluid has been considered by [11]. Intravascular plaque and other waste substances which are accumulated inside and on the wall of blood vessels restricted the flow of blood [3]. Herschel Bulkley fluid could be a better representation of blood as compared to the Bingham Plastic fluid and Power-law fluid [1]. Casson and Herschel Bulkley fluids exhibit better fluid flow behavior in arteries of 0.1 mm diameter, while in lower diameter (below 0.065mm) arteries, Herschel Bulkley fluid recommended the more [6].

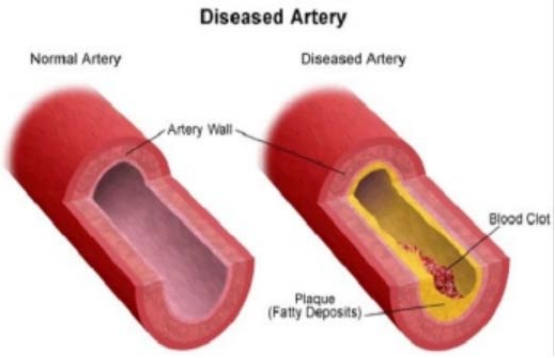

Fig. 1 Stenosis formation inside the artery

Corresponding Author: Dr. Chhama Awasthi*, *Department of Mathematics, Dr. APJ Abdul Kalam Technical University, Lucknow-226031, Uttar Pradesh, India.

It is to be noted that Power-law, Bingham Plastic, and Newtonian fluids are the general case of Herschel Bulkley fluid and these fluids can be obtained from Herschel Bulkley fluid by selecting the appropriate range of parameters. Blood represents non-Newtonian behavior in the diseased state [2]. The portrayal of Casson and Herschel Bulkley fluids are almost similar, but in the medium range of shear rate, Casson fluid is more suitable for blood assumption [9]. Bingham plastic fluid exhibits more significant information about blood rheology [4], [5]. The effect of unsteady blood flow through a tube with axisymmetric and non-symmetric stenosis was considered in [12]. Sankar and Lee [8] presented the non-Newtonian pulsatile fluid flow model through stenosed arteries under the body acceleration's effect. Body acceleration affects fluid characteristics like axial velocity, wall shear stress, flow rate, and resistance has revealed by Nagarani and Sarojamma [7].

The comparative study of non-Newtonian pulsatile blood flow through an inclined stenosed artery has been investigated. Here (Siddiqui and Chhama, [10]), work has been considered for Herschel Bulkley fluid. Bingham Plastic and Casson fluid have been considered for blood assumption. A comparison of the various flow behavior patterns of these fluids has been done in this model. Nanoparticles and peripheral layer thickness can be studied as the alternate case of this model.

II. MATHEMATICAL MODEL

Consider a laminar, unsteady, fully developed, axially symmetric blood flow along the axial direction z' in a stenosed inclined arterial segment, under the slip condition applied at the wall and body acceleration (see Fig. 1(a)). Blood flow is irregular and pulsatile because of the pressure gradient, present in the stenosed artery. Let (r', ϕ', z') be the cylindrical polar coordinates, where r' represents the radial coordinate, ϕ' represents the azimuthal angle, and z' represents the axial coordinate.

The expression for the radius of the artery is [Young and Tsai [12]].

$$\left.\begin{aligned} \frac{R'(z')}{R_0'} &= 1-\eta'\left[L_s'^{(m-1)}\left(z'-d'\right)-\left(z'-d'\right)^m\right], \quad d'\le z'\le d'+L_s' \\ &= 1, \qquad\qquad\qquad\qquad \text{otherwise} \end{aligned}\right\} \tag{1}$$

Where $R'(z')$, R_0' denotes the radius of the stenosed artery and the normal artery. Here d', L_s' denotes the stenosis location and stenosis length inside the artery. Stenosis is radially symmetric at m = 2 and stenosis shape parameter is $m \ge 2$ has been considered in this study. Where the parameter η' is defined as

$$\eta' = \frac{\delta'}{R_0' L_s'^{m}} \frac{m^{m/(m-1)}}{(m-1)}$$

Where the maximum height of the stenosis is δ' at $z' = d' + L_s' / m^{1/(m-1)}$ such that $\delta' / R_0' << 1$.

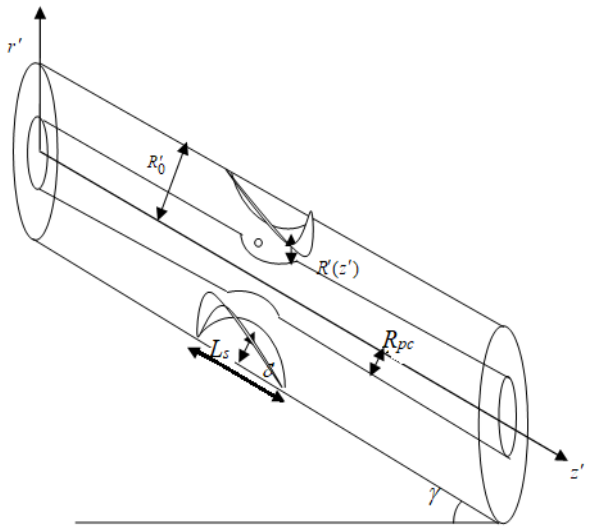

Fig. 1 (a) The geometry of an inclined artery with axially non-symmetric stenosis.

The momentum equations governing the fluid flow are simplified in equations (2) and (3) as (Schlichting and Gersten [15])

$$-\left(\frac{\partial p'}{\partial z'}\right)-\left(\frac{1}{r'}\right)\frac{\partial}{\partial r'}\left(r'\tau_s'\right)+B_a'(t')=\rho'\left\{\left(\frac{\partial v_a'}{\partial t'}\right)-g\sin\gamma\right\} \tag{2}$$

$$\frac{\partial p'}{\partial r'}=0 \tag{3}$$

Where γ indicates the inclination angle, v_a' indicates the axial velocity along z' direction, g indicates the acceleration due to gravity, ρ' indicates the density, P' indicates the pressure, t' indicates the time, τ_s' indicates the wall shear stress.

Also, $B_a'(t')$ indicates the periodic body acceleration in the axial direction, mathematically equation (4) expresses this body acceleration.

$$B_a'(t')=a_0\cos\left(\omega_{ba}'t'+\phi\right) \tag{4}$$

Where the symbol a_0 denotes the amplitude of body acceleration and ϕ denotes the phase angle of body acceleration with respect to the pressure gradient. $\omega_{ba}'=2\pi f_b'$ here f_b' denotes the frequency (in Hz). Also, we can assume the small f_b', so that the wave effect may be neglected.

The pressure gradient is expressed below

$$\frac{-\partial p'}{\partial z'}\left(z',t'\right)=A_0+A_1\cos\left(\omega_{pa}'t'\right),\quad t'\geq 0 \tag{5}$$

Where A_1 indicates the amplitude of the fluctuating component, A_0 indicates the pressure gradient in steady-state, and both the functions A_1, A_0 are functions of z'. Here ω'_{pa} indicates the frequency of oscillation of the unsteady flow and $\omega_{pa}'=2\pi f_p'$, with f_p' as the pulse rate frequency. Also, neglecting the radial velocity as it has a small magnitude.

The constitutive equation of Bingham Plastic fluid is

$$\begin{cases}\tau_s'=\theta_y'+\mu_0'\left(-\dfrac{\partial v_a'}{\partial r'}\right), & \text{if } \tau_s'\geq\theta_y'\\ \dfrac{\partial v_a'}{\partial r'}=0, & \text{if } \tau_s'<\theta_y'\end{cases} \tag{6}$$

The constitutive equation of Casson fluid is

$$\begin{cases}\sqrt{\tau_s'}=\sqrt{\theta_y'}+\sqrt{\mu_0'\left(-\dfrac{\partial v_a'}{\partial r'}\right)}, & \text{if } \tau_s'\geq\theta_y'\\ \dfrac{\partial v_a'}{\partial r'}=0, & \text{if } \tau_s'<\theta_y'\end{cases} \tag{7}$$

Where θ_y' indicates the viscosity and μ_0' indicates the yield stress of fluid. The velocity gradient vanishes in the core region (i.e. $\tau_s'<\theta_y'$), shows the plug flow region, and fluid flow behavior has been observed in the region $\tau_s'\geq\theta_y'$.

The boundary conditions are

i) At $r'=0$ τ_s' is finite. (8)

ii) At $r'=R'\left(z'\right)$, $v_a'=v_{as}'$ (9)

Where v_{as}' indicates the axial slip velocity at the obstructed wall of the artery.

Considering the following dimensionless variables:

$$\left.\begin{aligned} &r = r'/R_0',\ d = d'/R_0',\ t = t'\omega_{pa}',\ z = z'/R_0',\ \ \omega = \omega_{ba}'/\omega_{pa}',\ R(z) = R'(z')/R_0',\ R_{pc} = R_{pc}'(z')/R_0',\ F = A_0/4\rho' g,\ \delta = \delta'/R_0',\\ &e = A_1/A_0,\ v_a = \frac{4v_a'\mu_0'}{A_0 R_0'^2},\ v_{as} = \frac{4v_{as}'\mu_0'}{A_0 R_0'^2},\ \tau_s = \frac{\tau_s'}{A_0 R_0'/2},\ \alpha^2 = \frac{R_0'^2\omega_{pa}'\rho'}{\mu_0'},\ B = a_0/A_0,\ \theta_y = \frac{\theta_y'}{A_0 R_0'/2} \end{aligned}\right\} \quad (10)$$

Where α indicates the pulsatile Reynolds number.

With the help of non-dimensional variables, equation (2) can be written as

$$\alpha^2\left(\frac{\partial v_a}{\partial t}\right) = 4\left(1+\mathrm{e}\cos\mathrm{t}\right) + 4B\cos\left(\omega t+\phi\right) - \left(\frac{2}{r}\right)\frac{\partial}{\partial r}\left(r\tau_s\right) + \frac{\sin\gamma}{F} \quad (11)$$

Bingham Plastic fluid's constitutive equation in non-dimensionalize form is

$$\begin{cases} \tau_s = \theta_y + \frac{1}{2}\left(-\frac{\partial v_a}{\partial r}\right), & \text{if } \tau_s \geq \theta_y \\ \frac{\partial v_a}{\partial r} = 0, & \text{if } \tau_s < \theta_y \end{cases} \quad (12)$$

Casson fluid's constitutive equation in non-dimensionalize form is

$$\begin{cases} \sqrt{\tau_s} = \sqrt{\theta_y} + \sqrt{\frac{1}{2}}\sqrt{\left(-\frac{\partial v_a}{\partial r}\right)}, & \text{if } \tau_S \geq \theta_y \\ \frac{\partial v_a}{\partial r} = 0, & \text{if } \tau_S < \theta_y \end{cases} \quad (13)$$

The non-dimensionalize form of boundary conditions (8), (9) are

i) At $r = 0$, τ_s is finite (14)

ii) At $r = R(z)$, $v_a = v_{as}$ (15)

The stenosis geometry in dimensionless form is

$$\left.\begin{aligned} R(z) &= 1-\eta\left[L_s^{m-1}(z-d)-(z-d)^m\right], && d \leq z \leq d+L_s \\ &= 1, && \text{otherwise} \end{aligned}\right\} \quad (16)$$

The volumetric flow rate in the dimensionless form is defined below

$$Q(z,t) = 4\int_0^{R(z)} \mathrm{v}_a(z,r,t)\,r\,dr \quad (17)$$

$$\text{Where } Q(z,t) = \frac{Q'(z',t')}{\pi A_0\left(R_0'\right)^4/8\mu_0'}; \quad (18)$$

$Q'(z',t')$ denotes the volumetric flow rate.

III. ANALYSIS OF THE MODEL

Now we expand equations (11)-(13) about α^2 as non-dimensionalize equations (11)-(13) have α^2 term which is time-dependent. The axial velocity v_a, wall shear stress τ_s, plug core radius R_{pc}, plug core velocity v_{pc}, and plug core shear stress τ_{pc} in terms of α^2 (where $\alpha^2 << 0$) are expressed as follows.

$$v_a(z,r,t) = v_{0a}(z,r,t) + \alpha^2 v_{1a}(z,r,t) + ... \quad (19)$$

$$\tau_s(z,r,t) = \tau_{0s}(z,r,t) + \alpha^2\tau_{1s}(z,r,t) + ... \quad (20)$$

$$R_{pc}(z,t) = R_{0pc}(z,t) + \alpha^2 R_{1pc}(z,t) + ... \quad (21)$$

$$v_{pc}(z,t) = v_{0pc}(z,t) + \alpha^2 v_{1pc}(z,t) + ... \quad (22)$$

$$\tau_{pc}(z,t) = \tau_{0pc}(z,t) + \alpha^2\tau_{1pc}(z,t) + ... \quad (23)$$

With the use of equations (19) and (20) in equation (11) and equating the constant terms and α^2 terms, we get

$$\frac{\partial}{\partial r}\left(r\tau_{0s}\right)= 2r\left[\left(1+e\cos t\right)+B\cos\left(\omega t+\phi\right)+\frac{\sin\gamma}{4F}\right] \tag{24}$$

$$\frac{\partial v_{0a}}{\partial t} = -\frac{2}{r}\frac{\partial}{\partial r}\left(r\tau_{1s}\right) \tag{25}$$

Integrating equation (24) between 0 and R_{0pc}, using boundary condition (14)

$$\tau_{0\,pc} = R_{0\,pc}K(t) \tag{26}$$

where $\mathrm{K}(t) = \left[\left(1+e\cos t\right)+B\cos\left(\omega t+\phi\right)+\frac{\sin\gamma}{4F}\right]$

Integrating equation (24) between r and R_{0pc}, and using equations (14) and (26)

$$\tau_{0s} = rK(t) \tag{27}$$

Using equations (19) and (20), in constitutive equations (12) and (13)

Bingham model gives

$$\frac{\partial v_{0a}}{\partial r} = 2\left[\theta_y - \tau_{0s}\right] \tag{28}$$

$$\frac{\partial v_{1a}}{\partial r} = -2\tau_{1s} \tag{29}$$

Casson model gives

$$\frac{\partial v_{0a}}{\partial r} = -2\left[\tau_{0s}+\theta_y-2\sqrt{\tau_{0s}\theta_y}\right] \tag{30}$$

$$\frac{\partial v_{1a}}{\partial r} = -2\tau_{1s}\left[1-\sqrt{\frac{\theta_y}{\tau_{0s}}}\right] \tag{31}$$

Applying the expansion of v_a and τ_s from equations (19) and (20) in boundary equations (14) and (15) we have

i) At $r = 0$, τ_{0s}, τ_{1s} are finite (32)

ii) At $r = R(z)$, $v_{0a} = v_{as}, v_{1a} = 0$ (33)

Integrating equation (28) between r and R, and by using equations (27) and (33), we have v_{0a} of Bingham model is

$$v_{0a} = v_{as} + K(t)\left(R^2-r^2\right)-2\theta_y(R-r) \tag{34}$$

From equation (34), the first approximation v_{0pc} of the plug core velocity of the Bingham model can be obtained as

$$v_{0\,pc} = v_{as} + K(t)\left(R^2-R_{0\,pc}^2\right)-2\theta_y(R-R_{0\,pc}) \tag{35}$$

Now integrating equation (30) between r and R, and by using equations (27) and (33), we have v_{0a} of the Casson model as

$$v_{0a} = v_{as} + K(t)R^2\left[1-\left(\frac{r}{R}\right)^2+2d_1\left\{1-\left(\frac{r}{R}\right)\right\}-\frac{8}{3}\sqrt{d_1}\left\{1-\left(\frac{r}{R}\right)^{3/2}\right\}\right] \tag{36}$$

where $d_1 = \frac{\theta_y}{RK(t)}$

From equation (36), the first approximation v_{0p} of the plug core velocity of the Casson model is as follows

$$v_{0pc} = v_{as} + K(t)R^2\left[1-\left(\frac{R_{0pc}}{R}\right)^2 + 2d_1\left\{1-\left(\frac{R_{0pc}}{R}\right)\right\} - \frac{8}{3}\sqrt{d_1}\left\{1-\left(\frac{R_{0pc}}{R}\right)^{3/2}\right\}\right] \tag{37}$$

Using equations (34), (35) and boundary conditions (32), (33) in equation (25) we get the solutions for τ_{1s}, τ_{1pc} for the Bingham model as

$$\tau_{1s} = \frac{rK'(t)(r^2-2R^2)}{8} \tag{38}$$

$$\tau_{1pc} = \frac{R_{0pc}K'(t)(R_{0pc}^2-R^2)}{4} \tag{39}$$

Using equations (36), (37) and boundary conditions (32), (33) in equation (25) we get the solutions for τ_{1s}, τ_{1pc} for the Casson model as

$$\tau_{1s} = \left[\left\{\frac{\sqrt{d_1}R^2}{3} - \frac{R^2}{4}\right\}r + \frac{r^3}{8} - \frac{4}{21}\sqrt{d_1}R^{1/2}r^{5/2}\right]K'(t) \tag{40}$$

$$\tau_{1pc} = R_{0pc}\left[\frac{\sqrt{d_1}R^{1/2}}{3K'(t)}(R^{3/2}-{R_{0pc}}^{3/2}) - \frac{1}{4}(R^2-{R_{0pc}}^2)\right]K'(t) \tag{41}$$

From equation (29) and equation (38), v_{1a} and v_{1pc} for the Bingham model is

$$v_{1a} = \frac{K'(t)}{4}\left[r^2R^2 - \frac{(r^4+3R^4)}{4}\right] \tag{42}$$

$$v_{1pc} = \frac{K'(t)}{4}\left[R_{0pc}^2R^2 - \frac{(R_{0pc}^4+3R^4)}{4}\right] \tag{43}$$

With the help of equations (34), (35) and (42), (43) in (19) and (22), the axial velocity v_a and plug core velocity v_{pc} for the Bingham model is

$$v_a = v_{as} + K(t)\left(R^2-r^2\right) - 2\theta_y(R-r) + \alpha^2\frac{K'(t)}{4}\left[r^2R^2 - \frac{(r^4+3R^4)}{4}\right] \tag{44}$$

$$v_{pc} = v_{as} + K(t)\left(R^2-R_{0pc}^2\right) - 2\theta_y(R-R_{0pc}) + \alpha^2\frac{K'(t)}{4}\left[R_{0pc}^2R^2 - \frac{(R_{0pc}^4+3R^4)}{4}\right] \tag{45}$$

From equations (27), (31), and (40), v_{1a} and v_{1pc} for the Casson model is

$$v_{1a} = K'(t)R^4\left[\frac{1}{4}\left(\frac{r}{R}\right)^2 - \frac{1}{16}\left(\frac{r}{R}\right)^4 + d_1\left\{\begin{matrix}\frac{4}{9}\left(\frac{r}{R}\right)^{3/2} \\ -\frac{8}{63}\left(\frac{r}{R}\right)^3 - \frac{20}{63}\end{matrix}\right\} + \sqrt{d_1}\left\{\begin{matrix}\frac{53}{294}\left(\frac{r}{R}\right)^{7/2} - \frac{1}{3}\left(\frac{r}{R}\right)^{3/2} \\ -\frac{1}{3}\left(\frac{r}{R}\right)^2 + \frac{143}{294}\end{matrix}\right\} - \frac{3}{16}\right] \tag{46}$$

$$v_{1pc} = K'(t)R^4\left[\frac{1}{4}\left(\frac{R_{0pc}}{R}\right)^2 - \frac{1}{16}\left(\frac{R_{0pc}}{R}\right)^4 - \frac{3}{16} + d_1\left\{\begin{matrix}\frac{4}{9}\left(\frac{R_{0pc}}{R}\right)^{3/2} - \frac{20}{63} \\ -\frac{8}{63}\left(\frac{R_{0pc}}{R}\right)^3\end{matrix}\right\} + \sqrt{d_1}\left\{\begin{matrix}\frac{53}{294}\left(\frac{R_{0pc}}{R}\right)^{7/2} + \frac{143}{294} \\ -\frac{1}{3}\left(\frac{R_{0pc}}{R}\right)^2 - \frac{1}{3}\left(\frac{R_{0pc}}{R}\right)^{3/2}\end{matrix}\right\}\right] \tag{47}$$

With the help of equations (36), (37) and (46), (47) in equations (19) and (22), the axial velocity v_a , plug core velocity v_{pc} for the Casson model is

$$v_a = v_{as} + K(t)R^2\left[1-\left(\frac{r}{R}\right)^2 - \frac{8}{3}\sqrt{d_1}\left\{1-\left(\frac{r}{R}\right)^{3/2}\right\} + 2d_1\left\{1-\left(\frac{r}{R}\right)\right\}\right]$$
$$+\alpha^2 K'(t)R^4\left[\frac{1}{4}\left(\frac{r}{R}\right)^2 - \frac{1}{16}\left(\frac{r}{R}\right)^4 - \frac{3}{16} + d_1\left\{\begin{matrix}\frac{4}{9}\left(\frac{r}{R}\right)^{3/2} - \frac{20}{63} \\ -\frac{8}{63}\left(\frac{r}{R}\right)^3\end{matrix}\right\} + \sqrt{d_1}\left\{\begin{matrix}\frac{53}{294}\left(\frac{r}{R}\right)^{7/2} - \frac{1}{3}\left(\frac{r}{R}\right)^{3/2} \\ -\frac{1}{3}\left(\frac{r}{R}\right)^2 + \frac{143}{294}\end{matrix}\right\}\right] \tag{48}$$

$$v_{pc} = v_{as} + K(t)R^2\left[1-\left(\frac{R_{0pc}}{R}\right)^2 - \frac{8}{3}\sqrt{d_1}\left\{1-\left(\frac{R_{0pc}}{R}\right)^{3/2}\right\} + 2d_1\left\{1-\left(\frac{R_{0pc}}{R}\right)\right\}\right]$$
$$+\alpha^2 K'(t)R^4\left[\frac{1}{4}\left(\frac{R_{0pc}}{R}\right)^2 - \frac{1}{16}\left(\frac{R_{0pc}}{R}\right)^4 - \frac{3}{16} + d_1\left\{\begin{matrix}\frac{4}{9}\left(\frac{R_{0pc}}{R}\right)^{3/2} - \frac{20}{63} \\ -\frac{8}{63}\left(\frac{R_{0pc}}{R}\right)^3\end{matrix}\right\} + \sqrt{d_1}\left\{\begin{matrix}\frac{53}{294}\left(\frac{R_{0pc}}{R}\right)^{7/2} - \frac{1}{3}\left(\frac{R_{0pc}}{R}\right)^{3/2} \\ -\frac{1}{3}\left(\frac{R_{0pc}}{R}\right)^2 + \frac{143}{294}\end{matrix}\right\}\right] \tag{49}$$

Neglecting α^2 terms and higher powers of α terms from equation (21), and with the use of equation (26), R_{0pc} term of R_{pc} is

$$r\big|_{\tau_{opc}=\theta_y} = R_{0pc} = \frac{\theta_y}{K(t)} \tag{50}$$

Using equations (26), (27) and (38), (39) in equations (20) and (23), the wall shear stress τ_s, τ_p for the Bingham model is

$$\tau_s = RK(t) - \frac{\alpha^2 K'(t)R^3}{8} \tag{51}$$

$$\tau_{pc} = R_{0pc}K(t) + \frac{\alpha^2 R_{0pc}K'(t)(R_{0pc}^2 - R^2)}{4} \tag{52}$$

Using equations (26), (27) and (40), (41) in equations (20) and (23), the wall shear stress τ_s, τ_p for the Casson model is

$$\tau_s = RK(t) - \alpha^2\left[\left\{\frac{\sqrt{d_1}R^2}{3} - \frac{R^2}{4}\right\}r + \frac{r^3}{8} - \frac{4}{21}\sqrt{d_1}R^{1/2}r^{5/2}\right]K'(t) \tag{53}$$

$$\tau_{pc} = R_{0pc}K(t) + \alpha^2 R_{0pc}\left[\frac{\sqrt{d_1}R^{1/2}}{3K'(t)}(R^{3/2} - {R_{0pc}}^{3/2}) - \left(\frac{1}{4}\right)(R^2 - {R_{0pc}}^2)\right]K'(t) \tag{54}$$

With the help of equation (17) and expression of axial velocity of Bingham Plastic fluid and Casson fluid, we get volumetric flow rate Q_b for Bingham model and Q_c for Casson model as

$$Q_b = 2R^2 v_{as} - \frac{4}{3}\theta_y\left(R^3 - R_{0pc}^3\right) + \left(R^4 - R_{0pc}^4\right)K(t) - \frac{\alpha^2 K'(t)}{12}\left\{(R_{0pc}^6 + 2R^6) - 3R_{0pc}^4 R^2\right\} \tag{55}$$

$$Q_c = Q_{1c} + Q_{2c} + Q_{3c} + Q_{4c} \tag{56}$$

where

$$Q_{1c} = 2R_{0pc}^2 v_{as} + 2K(t)R^2R_{0pc}^2 + 4d_1K(t)R^2R_{0pc}^2\left\{1-(R_{0pc}/R)\right\} - (1\ 6/3)R^2R_{0pc}^2\sqrt{d_1}\left\{1-(R_{0pc}/R)^{3/2}\right\}$$

$$Q_{2c} = 2R^2v_{as}\left\{1-(R_{0pc}/R)^2\right\} + K(t)R^4\left\{1-2(R_{0pc}/R)^2-(R_{0pc}/R)^4\right\} - K(t)R^4\sqrt{d_1}\left\{(160/21)-(32/3)(R_{0pc}/R)^2+(64/21)(R_{0pc}/R)^{7/2}\right\}$$
$$+4d_1K(t)R^4\left\{1-(R_{0pc}/R)^2\right\} - (8/3)d_1K(t)R^3\left\{1-(R_{0pc}/R)^3\right\}$$

$$Q_{3c} = 2\alpha^2K'(t)R^2R_{0pc}^4\left\{1-(1/4)(R_{0pc}/R)^2\right\} - (3/8)\alpha^2K'(t)R^4R_{0pc}^2 + \alpha^2(1/147)K'(t)R^4R_{0pc}^2\sqrt{d_1}\left\{143+53(R_{0pc}/R)^{7/2}\right\}$$
$$+\alpha^2(8/9)K'(t)R^{5/2}R_{0pc}^{7/2}d_1\left\{1-(2/7)(R_{0pc}/R)^{3/2}\right\}$$

$$Q_{4c} = \alpha^2K'(t)R^6\left\{(3/8)(R_{0pc}/R)^2-(1/4)(R_{0pc}/R)^4+(1/24)(R_{0pc}/R)^6-(1/6)\right\} + \alpha^2K'(t)R^6\sqrt{d_1}\left\{\begin{array}{l}(49/33)-(212/1617)(R_{0pc}/R)^{11/2}\\-(143/147)(R_{0pc}/R)^2-(8/21)(R_{0pc}/R)^{7/2}\end{array}\right\}$$

Neglecting higher powers of α terms and α^4 terms from the equation (21), the R_{1pc} term of the plug core radius is

$$R_{1pc} = \frac{\tau_1\left(R_{0pc}\right)}{K(t)} \tag{57}$$

With the help of equations (21), (39), and (50), the R_{pc} for Bingham model is

$$R_{pc} = \frac{\theta_y}{K(t)} + \frac{\alpha^2 R_{0pc}K'(t)(R_{0pc}^2-R^2)}{4} \tag{58}$$

With the help of equations (21), (41), and (50), the R_{pc} for Casson model is

$$R_{pc} = \frac{\theta_y}{K(t)} + \frac{\alpha^2K'(t)R_{0p}}{K(t)}\left[\frac{\sqrt{d_1}R^{1/2}}{3K'(t)}(R^{3/2}-{R_{0pc}}^{3/2}) - \left(\frac{1}{4}\right)(R^2-{R_{0pc}}^2)\right] \tag{59}$$

In dimensionless form, the effective viscosity for the Bingham model and Casson model, with the help of equations (18), (55), and (56) can be obtained as

$$\mu_b = \left(R(z)\right)^4\left(1+e\cos t\right)\left\{Q_b\right\}^{-1} \tag{60}$$

$$\mu_c = \left(R(z)\right)^4\left(1+e\cos t\right)\left\{Q_{1c}+Q_{2c}+Q_{3c}+Q_{4c}\right\}^{-1} \tag{61}$$

IV. RESULTS AND DISCUSSION

The significant results have been observed with the help of MATLAB, and some fixed parameters. (Young and Tsai [12]; D.W. Liepsch [13]; Ookwara and Ogowa [14]). Fig.2 shows the axial velocity versus radial distance graph under the effect of γ and v_{as}, for different fluids with the use of fixed values $\delta = 0.1$, $F = 0.2$, $\phi = 0.2$, $n = 0.95$, $\omega = 1$, e = 1, $m = 2$, $\alpha = 0.2$, t = 1. From Fig. 2 it has been analyzed that the v_{as} and γ augmented the axial velocities of all fluids, and the axial velocity profile of Herschel Bulkley fluid is more than Casson fluid while less than Bingham Plastic fluid in an obstructed artery. Fig.3 shows the variation of δ on the axial velocity and radial distance graph with the use of values $B = 1$, $F = 0.2$, $n = 0.95$, $\alpha = 0.2$, e = 1, $\omega = 1$, $m = 2$, $t = 1$, $v_{as} = 0.1$ for different fluids. It has been found that in the stenosed artery, the velocity of Bingham Plastic fluid is more than that of Herschel Bulkley fluid and Casson fluid. Fig.3 also reveals that the velocity of all fluids diminishes as stenosis height increases. Fig.4 depicts the axially non symmetric stenosis shape effect on axial velocity versus radial distance graph for different fluids and for fixed values $\gamma = 30^0$, $\theta_y = 0.1$, $F = 0.2$, $\alpha = 0.2$, e = 1, $n = 0.95$, $\omega = 1$, $t = 1$, $v_{as} = 0.1$ Fig.4 reveals that as stenosis shape rises from $m = 2$ to $m = 10$, axial velocity hikes. Fig.5 sketches the time and the plug core velocity graph for $\gamma = 30^0$, $F = 0.2$, $\phi = 0.2$, e = 0.05, $\delta = 0.1$, $\omega = 1$, $n = 0.95$ for different fluids. It has been optimized that in the core region, the velocity of Bingham Plastic fluid is more, in comparison to Casson fluid whereas less, in comparison to Herschel Bulkley fluid.

Also, velocity diminishes very slightly as time rises from 0 to 3 and then velocity rises as time rises from 3 to 6.

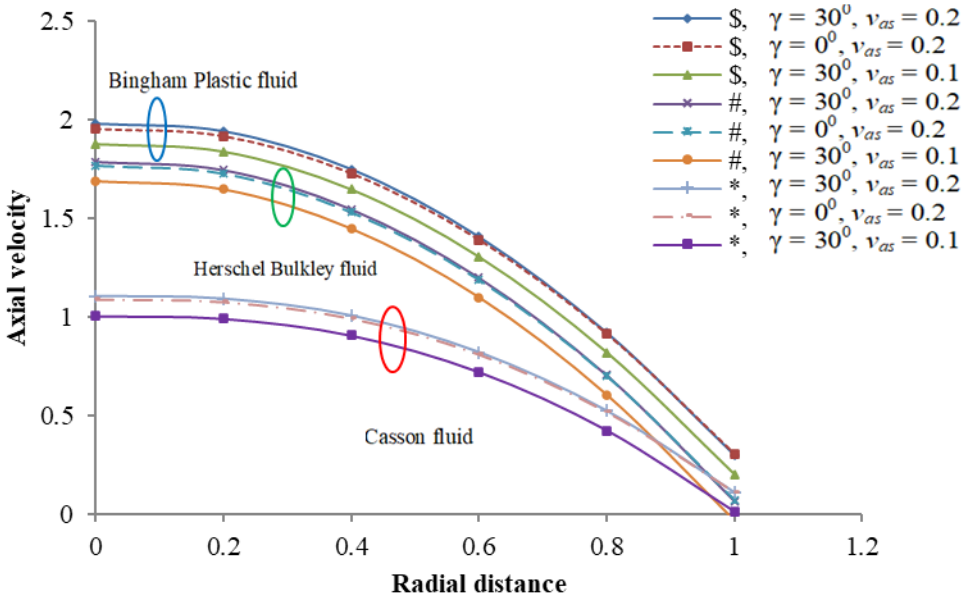

Fig.2 Variation of axial velocity with the radial distance for different values of inclined angle and slip, * shows Casson fluid, # shows Herschel Bulkly fluid, $ shows Bingham Plastic fluid.

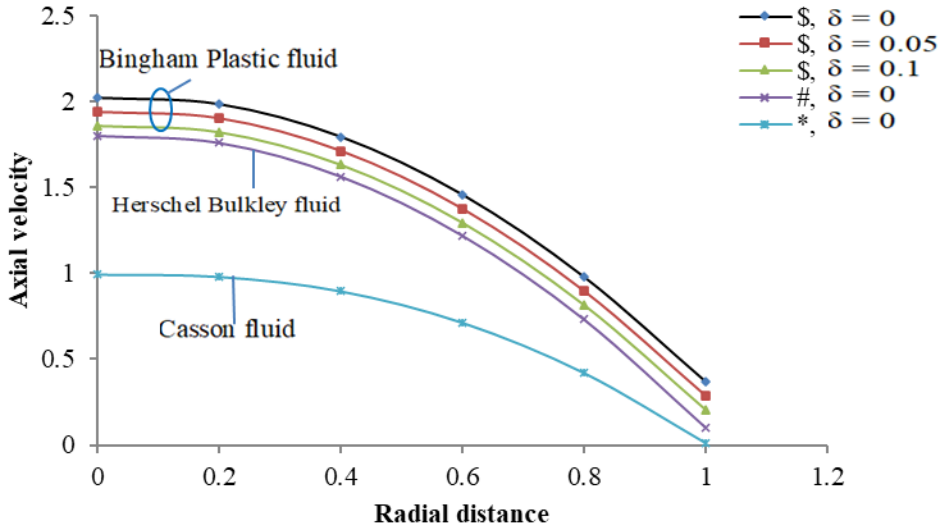

Fig. 3 Variation of axial velocity with the radial distance for different values of stenosis height, * shows Casson fluid, # shows Herschel Bulkley fluid, $ shows Bingham Plastic fluid.

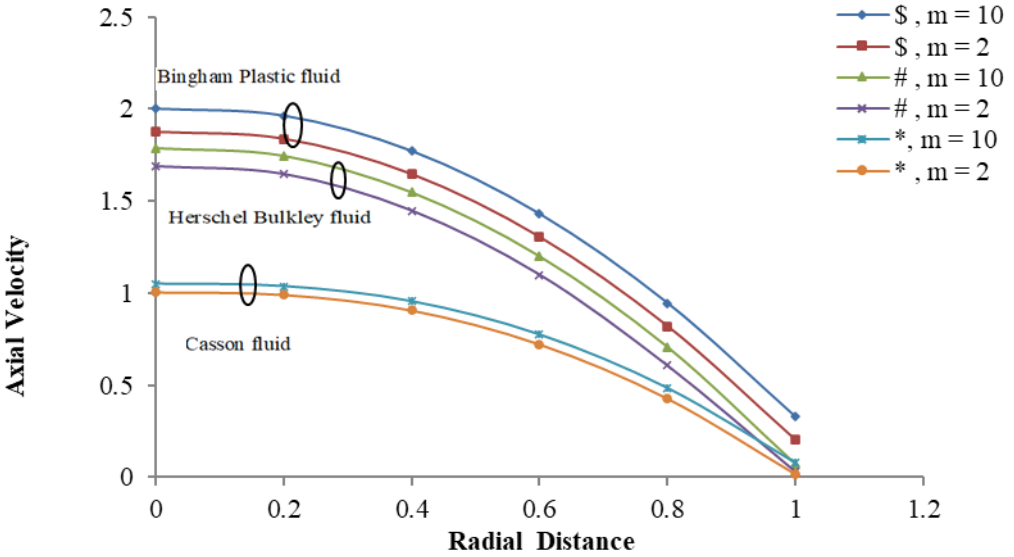

Fig.4 Variation of axial velocity with the radial distance for different values of shape parameter, * shows Casson fluid, # shows Herschel Bulkley fluid, $ shows Bingham Plastic fluid.

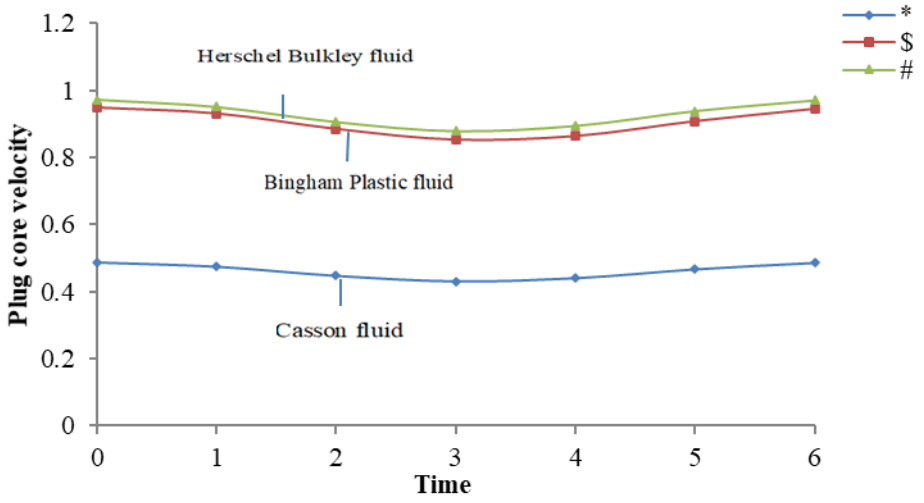

Fig.5 Variation of plug core velocity with time ,* shows Casson fluid, # shows Herschel Bulkley fluid, $ shows Bingham Plastic fluid.

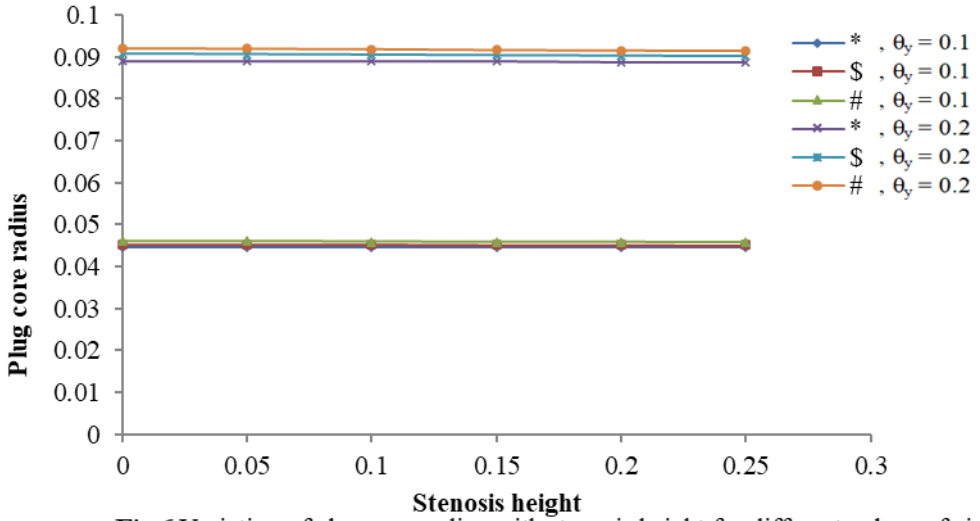

Fig.6 Variation of plug core radius with stenosis height for different values of yield stress, * shows Casson fluid, # shows Herschel Bulkley fluid,$ shows Bingham

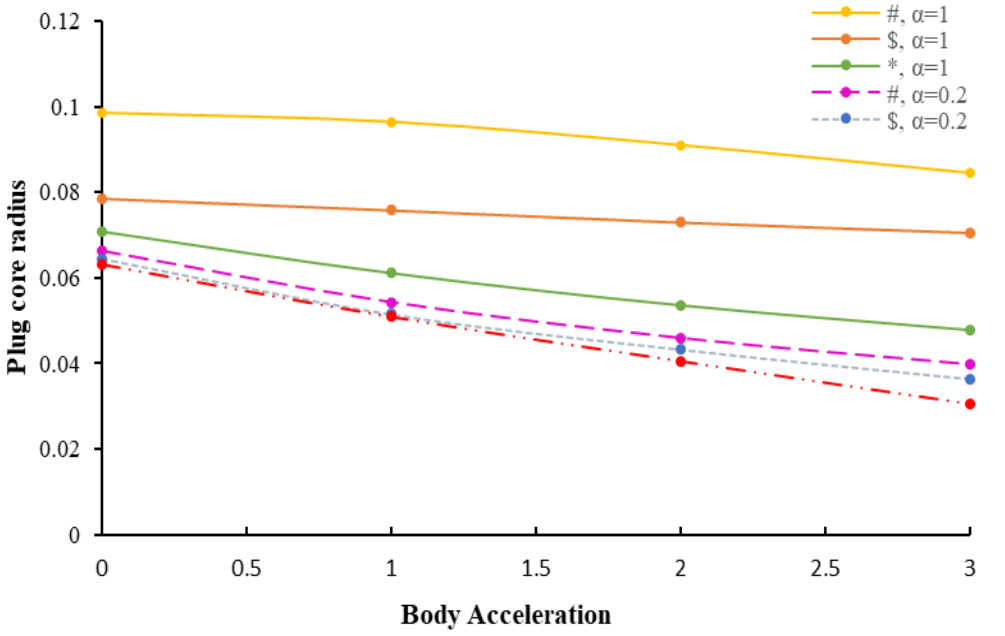

Fig. 7. Variation of plug core radius with stenosis height for different values of yield stress, * shows Casson fluid, # shows Herschel Bulkley fluid,$ shows Bingham Plastic fluid.

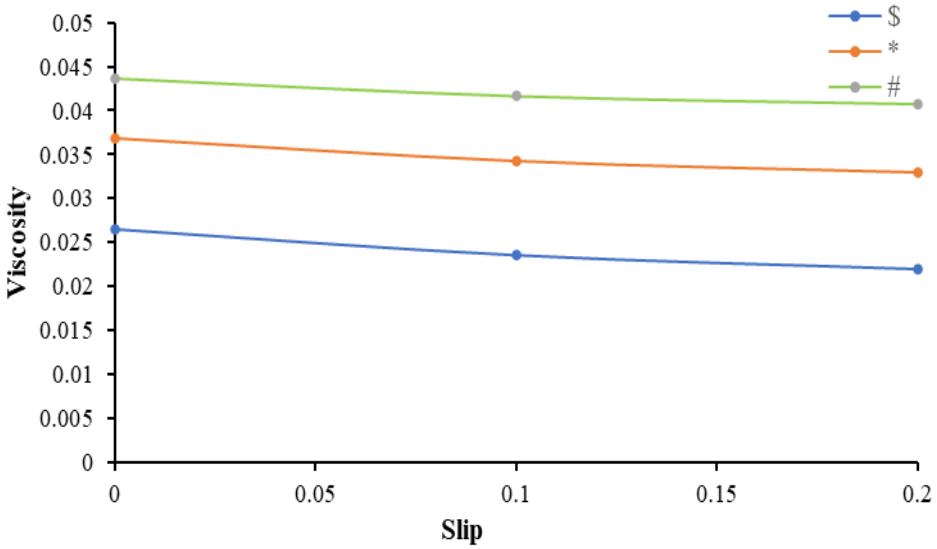

Fig. 8. Variation of Viscosity with slip for different values of shape parameter, * shows Casson fluid, # shows Herschel Bulkley fluid, $ shows Bingham Plastic fluid.

Fig.6 shows the stenosis height and plug core radius graph and Fig. 7 describes the body acceleration and plug core radius variation, for different fluids to check the impact of θ_y and α values for the fixed values F = 0.2, n = 0.95, ϕ = 0.2, e = 1, δ = 0.1, ω = 1, t = 1. Fig.6 and Fig. 7 shows that the plug core radius of Bingham Plastic fluid is greater in comparison to Casson fluid while less in comparison to Herschel Bulkley fluid. Fig. 6 reveals, plug core radius minimizes, on rising the stenosis height value. Whereas Fig. 7 illustrated that increasing the Reynolds number hikes the plug core radius. Also, Fig. 6 and Fig. 7 explain that raising the stenosis height and body acceleration minimizes the plug core radius. Fig. 8 shows the variation of viscosity with slip for different fluids. It has been observed that the viscosity of Casson fluid is greater than Herschel Bulkley fluid but lesser than Bingham Plastic fluid on increasing the slip.

V. CONCLUSION

This study investigated the blood rheology of non-Newtonian fluid. The following significant remarks have been concluded here as

1. It has been found, that the axial velocity of Herschel Bulkley fluid is more in comparison to Casson fluid while lower in comparison to Bingham Plastic fluid in normal as well as in obstructed artery.
2. Slip velocity and inclination hike the axial velocity of all fluids while the increase of stenosis height reduces the velocity.
3. Change in stenosis shape parameter from $m = 2$ to $m = 10$, increases the velocity.
4. Plug core velocity increases on increasing the body acceleration. Plug velocity of Bingham Plastic fluid is greater in comparison to Casson fluid whereas less in comparison to Herschel Bulkley fluid.
5. Plug core radius of Bingham Plastic fluid is more in comparison to Casson fluid while less in comparison to Herschel Bulkley fluid.
6. The rise in yield stress and Reynolds number raises the plug core radius and a rise in stenosis height and body acceleration diminishes the plug core radius slightly.
7. Effective viscosity decreases as slip velocity increases for all the fluids and viscosity of Casson fluid is greater in comparison to Herschel Bulkley fluid while lesser than the Bingham Plastic fluid.

ACKNOWLEDGMENT

Author (Dr. Chhama Awasthi) is thankful to the TEQIP (SPFU, World Bank) at HBTU, Kanpur, India for awarding the fellowship for this research work.

REFERENCES

1. P. Chaturani, R. Ponnalagar Samy, A study of non-Newtonian aspects of blood flow through stenosed arteries and its applications in arterial diseases, *Biorheology*, 22 (1985), 521–531.
2. S. Chien, Hemorheology in clinical medicine. Recent Advances in Cardiovascular Diseases 2 (Suppl.), (1981), 21-26.
3. H. Dwyer, H., Cheer, A., Rutaganira, T. and Shacheraghi, N. 'Calculation of unsteady flows in curved pipes', *Journal of Fluids Engineering*, 123 (4), (2001), 869-877.
4. F.R. Eirich, *Rheology Theory and Applications*, 3, Academic Press Inc. Publishers, New York, S.F., London. (1960).
5. Y.C. Fung, *Biomechanics*, Springer-Verlag, New York, Heidelberg, Berlin, (1981).
6. N. Iida, Influence of plasma layer on steady blood flow in microvessels, Jpn. *J. Appl. Phys.* 17, (1978), 203–214.
7. P. Nagarani, Sarojamma G., 'Effect of body acceleration on a pulsatile flow of Casson fluid through a mild stenosed artery', *Korea-Australia Rheology*, 20(4) (2008), 189–196.
8. D.S. Sankar, U. Lee, Nonlinear mathematical analysis for blood flow in a constricted artery under periodic body acceleration, *Communications in Nonlinear Science and Numerical Simulation*, 16(11) (2011), 4390–4402.
9. G.W. Scott Blair, D. C. Spanner, *An Introduction to Biorheology*, Elsevier Scientific Publishing Company, Amsterdam, Oxford, and New York. (1974).
10. S.U. Siddiqui, C. Awasthi, Mathematical Modelling of Pulsatile Herschel Bulkley Fluid Flow through an Inclined Stenosed Artery, *Int. J. of Mathematical Archive* 8(7), (2017), 205-215.
11. C. Tu, M. Deville, Pulsatile flow of non-Newtonian fluids through arterial stenosis. J Biomech. 29, (1996), 899–908.
12. D.F. Young, F.Y. Tsai, Flow characteristics in models of arterial stenosis – II. Unsteady flow, *J. of Biomech.* 6(5) (1973), 547-559.
13. D.W. Liepsch, Flow in Tubes and Arteries—A Comparison. Biorheology, 23 (1986), 395-433.
14. S. Ookawara, K. Ogowa, Flow Properties of Newtonian and Non-Newtonian Fluid Downstream of Stenosis. Journal of Chemical Engineering Japan, 33 (2000), 582-590. https://doi.org/10.1252/jcej.33.582
15. H. Schlichting, K. Gersten, *Boundary layer theory*, Springer-Verlag, 2004.

Source of support: Nil, Conflict of interest: None Declared.